

Parametrization of C-shocks. Evolution of the Sputtering of Grains

I. Jiménez-Serra^{1,2}, P. Caselli^{2,3}, J. Martín-Pintado¹ and T. W. Hartquist²

¹ Departamento de Astrofísica Molecular e Infrarroja, Instituto de Estructura de la Materia (CSIC), C/ Serrano 121, E-28006 Madrid, Spain

² School of Physics and Astronomy, University of Leeds LS2 9JT, Leeds, United Kingdom

³ INAF-Osservatorio Astrofisico di Arcetri, Largo E. Fermi 5, I-50125 Firenze, Italy

Received September 15, 1996; accepted March 16, 1997

ABSTRACT

Context. The detection of a narrow SiO line emission toward the young shocks of the L1448-mm outflow has been interpreted as a signature of the magnetic precursor of C-shocks. In contrast with the very low SiO abundances ($\leq 10^{-12}$) derived from the ambient gas, the narrow SiO emission in the precursor component at almost ambient velocities reveals enhanced SiO abundances of $\sim 10^{-11}$. This enhancement has been proposed to be produced by the sputtering of the grain mantles at the very first stages of C-shocks. However, modelling of the sputtering of grains has usually averaged the SiO abundances over the dissipation region of C-shocks, which cannot explain the recent observations.

Aims. To model the evolution of the gas phase abundances of molecules like SiO, CH₃OH and H₂O, produced by the sputtering of the grain mantles and cores as the shock propagates through the ambient gas. We consider different initial gas densities and shock velocities.

Methods. We propose a parametric model to describe the physical structure of C-shocks as a function of time. Using the known sputtering yields for water mantles (with other minor constituents like silicon and CH₃OH) and olivine cores by collisions with H₂, He, C, O, Si, Fe and CO, we follow the evolution of the abundances of silicon, CH₃OH and H₂O ejected from grains along the evolution of the shock.

Results. The evolution of the abundances of the sputtered silicon, CH₃OH and H₂O shows that CO seems to be the most efficient sputtering agent in low velocity shocks. The velocity threshold for the sputtering of silicon from the grain mantles is appreciably reduced (by 5-10 km s⁻¹) by CO compared to other models. The sputtering by CO can generate SiO abundances of $\sim 10^{-11}$ at the early stages of low velocity shocks, consistent with those observed in the magnetic precursor component of L1448-mm. Our model satisfactorily reproduce the progressive enhancement of SiO, CH₃OH and H₂O observed in this outflow, suggesting that this enhancement may be due to the propagation of two shocks with $v_s = 30$ km s⁻¹ and $v_s = 60$ km s⁻¹ coexisting within the same region.

Conclusions. Our simple model can be used to estimate the time dependent evolution of the abundances of molecular shock tracers like SiO, CH₃OH, H₂O or NH₃ in very young molecular outflows.

Key words. ISM: clouds – physical processes: shock waves – ISM: jets and outflows – ISM: dust, extinction

1. Introduction

In young molecular outflows, it is expected that changes in the molecular emission could be observed due to the propagation of shocks into the ambient material. So far, the L1448-mm outflow is the only object where time variability of the SiO emission in the high velocity jet has been detected, indicating the presence of very young shocks (Girart & Acord 2001).

It is well known that silicon is heavily depleted onto the grain mantles and grain cores in the quiescent gas of molecular dark clouds like TMC-1, L183 and L1448 (SiO abundance of $\leq 10^{-12}$; Ziurys, Friberg & Irvine 1989; Martín-Pintado, Bachiller & Fuente 1992; Requena-Torres et al. 2007). The detection of large SiO abundances in regions with outflow activity is therefore a clear indicator of the destruction of dust grains by the interaction of magnetohydrodynamic (MHD) shock waves

(or C-shocks) with the ambient gas (Martín-Pintado et al. 1992; Flower et al. 1996; Caselli et al. 1997).

The typical SiO abundances measured in the high velocity gas of young molecular outflows like in L1448-mm (Martín-Pintado et al. 1992) are of $\geq 10^{-6}$, which implies an enhancement by more than 6 orders of magnitude with respect to the SiO abundances measured in the quiescent gas. The recent detection of very narrow SiO emission at almost ambient velocities toward this outflow has been proposed to be produced by the magnetic precursor of C-shocks (Jiménez-Serra et al. 2004). The SiO abundance of $\sim 10^{-11}$ for this narrow emission clearly contrasts with the large SiO enhancement found in the high velocity postshock gas, and with the much lower SiO abundance of the quiescent material.

Toward the young shocks of the L1448-mm outflow, Jiménez-Serra et al. (2005) have also reported an evolutionary trend of the SiO and CH₃OH abundances (methanol is

the most abundant molecule after H_2O in the grain mantles; Tielens & Allamandola 1987) to be enhanced from the ambient gas to the moderate velocity component, as if the grain mantles would have been progressively eroded by the recent interaction of low velocity shocks.

Modelling of C-shocks that includes only the sputtering of grain cores, shows that an appreciable fraction of silicon material starts to be ejected from grains for $v_s \geq 25\text{--}30 \text{ km s}^{-1}$ (Flower et al. 1996; Caselli et al. 1997; May et al. 2000). Although these models predict SiO abundances consistent with those observed in the postshock gas ($\sim 10^{-8}\text{--}10^{-7}$), the sputtering of SiO from the cores cannot reproduce the lower SiO abundances of $\sim 10^{-11}$ found in the narrow precursor component of L1448-mm.

Calculations of the sputtering yield of silicon by heavy atoms like C, O, Si and Fe on SiO_2 and olivine (MgFeSiO_4) cores show that, despite the low relative abundances of these species with respect to H_2 and He in dark clouds, these heavy particles can dominate the sputtering of grains at low shock velocities (Field et al. 1997; May et al. 2000). Furthermore, abundant molecules like CO could also play an important role in the sputtering of dust grains since these species can sputter like atoms of equivalent mass for low impact velocities (May et al. 2000). Considering that silicon could be a minor constituent of the mantles, their sputtering by these heavy species in low velocity shocks could efficiently erode them generating the SiO abundances observed for the narrow SiO line emission in L1448-mm. Up to date, the evolution of the sputtering of grains has not been studied in detail. The questions of which species are the most efficient sputtering agents, and which time-scales are needed to eject most of the silicon material from grains, still remain uncertain.

In this paper, we present a parametric model of C-shocks to describe in detail the time dependent evolution of the molecular abundances sputtered from grains in low and high velocity shocks. This approximation constitutes a powerful tool for interpreting the molecular abundances measured in young molecular outflows. In addition to H_2 and He, heavy atoms and molecules have been also considered as sputtering agents. In Sec. 2, we present the approximations used to describe the steady state profile of the physical structure of C-shocks. In Sec. 3, we show the procedure used to determine the sputtering of the grain mantles and the grain cores. In Sec. 4, we present the results of the sputtering of silicon from grains for several initial gas densities and shock velocities. In Sec. 5 and 6, we compare the sputtered SiO, CH_3OH and H_2O abundances with those measured in the L1448-mm outflow. The conclusions are finally summarized in Sec. 7.

2. The C-shock Structure in the Preshock Frame

We consider a plane-parallel C-shock that propagates through the quiescent gas with velocity v_s . As a first approximation, we have assumed steady state profiles for the evolution of the physical parameters in the shock. The validity of this approximation, versus more recent time-dependent modelling of the physical structure of C-shocks, will be discussed in detail in Sec. 4.1.

Table 1. Initial gas phase abundances of He, C, O, Si, Fe and CO.

Element/ Molecule	Abundance ^a [$n(\text{X})/n(\text{H})$]
He	0.1
C	7.1×10^{-9}
O	1.8×10^{-4}
Si	8.0×10^{-9}
Fe	3.0×10^{-9}
CO	1.5×10^{-4}

^a From the low metal case for dense cloud chemistry (Prasad & Huntress 1982; Herbst & Leung 1989; Graedel et al. 1982).

The initial H_2 density and temperature of the ambient cloud are n_0 and T_0 , respectively. Since one of the aims of this work is to directly compare our results with observations toward the young L1448-mm outflow, it is convenient to consider that the velocities of the ion and neutral fluids, v_i and v_n , are in the frame co-moving with the preshock gas. These velocities are approximated by:

$$v_{n,i} = (v_s - v_0) - \frac{(v_s - v_0)}{\cosh[(z - z_0)/z_{n,i}]} \quad (1)$$

where z is the spatial coordinate and the z_n/z_i ratio governs the strength of the velocity decoupling between the ion and neutral fluids. z_0 corresponds to the distance at which these fluids start to decouple (see Sec. 4.1 for details on how to estimate these parameters). An additional velocity, v_0 , also needs to be considered in the equations for v_n and v_i in order to avoid infinite compression of the far downstream gas (see Eq. 3 below). v_0 depends on the shock parameters and is defined as the final downstream velocity of the ion and neutral fluids *in the frame of the shock* (in the preshock frame, this final velocity would be $v_s - v_0$; see Sec. 4.1). As shown in Appendix A, this velocity is tightly linked to the shock and Alfvén velocities, v_s and v_A , through shock jump conditions.

The ion-neutral drift speed v_d is $v_d = |v_n - v_i|$, and the neutral fluid flow time is calculated as (see Eqs. A.7 and B.10):

$$t = \int \frac{dz}{v_s - v_n} \quad (2)$$

From the principle of mass conservation, the neutral density, n_n , is given by:

$$n_n = \frac{n_0 v_s}{v_s - v_n} \quad (3)$$

The temperature of the neutral fluid, T_n , is approximated by a Planck-like function as:

$$T_n = T_0 + \frac{[a_T (z - z_0)]^{b_T}}{\exp[(z - z_0)/z_T] - 1} \quad (4)$$

where b_T is an integer, and a_T and z_T are related to the maximum value of T_n ($T_{n,\text{max}}$) and the distance $z_{n,\text{max}}$ at which T_n

Table 2. Fractional abundances of H₂O, CH₃OH and Si/SiO assumed for the icy mantles and the grain cores.

Species	Abundances [χ]	
	Mantles	Cores
H ₂ O	$7.25 \times 10^{-5(a)}$...
CH ₃ OH	$\sim 10^{-6(b)}$...
Si/SiO	$\sim 10^{-8(b)}$	$\sim 3.6 \times 10^{-5(c)}$

(a) From Whittet & Duley (1991).

(b) From Jiménez-Serra et al. (2005).

(c) From Anders & Grevesse (1989) and Snow & Witt (1996).

reaches its maximum value. The temperature of the ion fluid is calculated by using $T_i = T_n + \left(\frac{m v_d^2}{3k}\right)$.

The comparison of the model predictions with observations (Secs. 5 and 6) requires the consideration of the radial velocity of the preshock gas (ambient cloud gas) relative to the observer, v_{cl} . This velocity, the radial velocity of the emission measured by the observer, v_{LSR} , and the velocity of the neutral fluid as measured in the frame of the ambient medium, v_n , are related by:

$$v_{LSR} = v_{cl} + v_n \quad (5)$$

In Appendix A, we also give the equations for v_n , v_i and n_n within the frame of the shock (see Eqs. A.1 and A.5) that will be used in Sec. 4.1 to validate this parametric approximation.

3. Sputtering of Grains

In this section, we describe the sputtering of grains produced by collisions with H₂ and He and other heavy atomic and molecular species such as C, O, Si, Fe and CO (see Appendix B for the full explanation of the method). Although we consider that most silicon is locked into the olivine grain cores, we assume that a small fraction of this element is also present within the icy water mantles ($q_m = 1.4 \times 10^{-4}$; see below). CH₃OH has been also considered as another constituent of the icy mantles.

3.1. Sputtering of the Grain Mantles

To study the sputtering of the grain mantles, we have followed the procedure described by Caselli et al. (1997). The sputtering rate per unit volume and grain (Eq. B.1 in Appendix B) has been derived by averaging the sputtering yield at low energies (Eq. B.2) over a velocity-shifted Maxwellian distribution characterized by T_n and v_d . The surface binding energy U_0 of the water mantles is of 0.53 eV (Tielens et al. 1994). The projectile masses m_p are 2, 4, 12, 16, 28, 56 and 28 amu for H₂, He, C, O, Si, Fe and CO, respectively. The target mass M_t is considered to be 18 amu which corresponds to the molecular mass of H₂O. The initial fractional abundances of He, C, O, Si, Fe and CO, relative to atomic hydrogen, are shown in Table 1. We assume that these abundances remain constant throughout the dissipation region of the shock. The volume

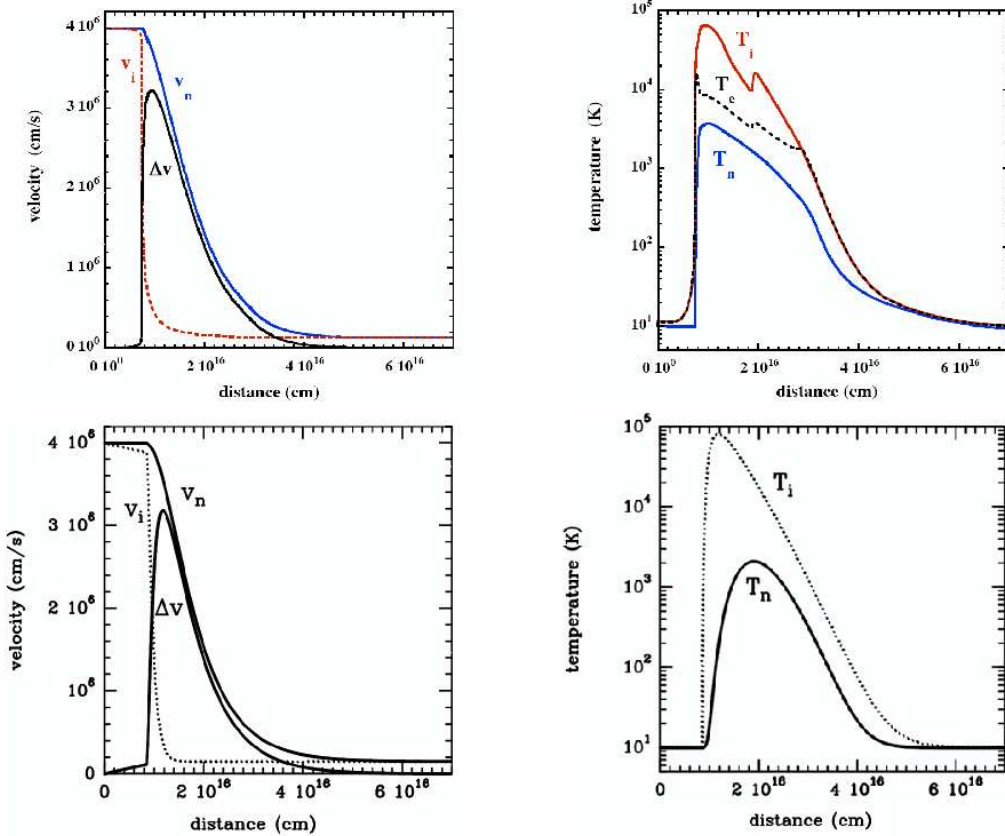
density of grains, n_g , is derived by considering a gas-to-dust mass ratio of ~ 100 , a constant grain radius of $0.1 \mu\text{m}$ and a density of the grain core material of 3.5 g cm^{-3} (most of the volume of a grain is filled by the silicate core; Caselli et al. 1997). The total sputtering rate for H₂O, CH₃OH and silicon are calculated with Eqs. (B.4), (B.5) and (B.6). The total volume densities of these species are finally estimated with Eqs. (B.7), (B.8) and (B.9). Since the amount of material contained within the grain mantles is limited, we assume that the maximum abundances of silicon and CH₃OH ejected from the mantles are those of SiO and CH₃OH measured in the low velocity gas of the L1448-mm outflow ($\sim 10^{-8}$ and $\sim 10^{-6}$, respectively; see Table 2 and Jiménez-Serra et al. 2005). From the observations, and assuming a H₂O abundance of $\sim 7.25 \times 10^{-5}$ (Table 2 and Whittet & Duley 1991), we can derive the fraction of silicon, q_m , and CH₃OH, r_m , present within the water mantles as $q_m = \chi(\text{SiO})/\chi(\text{H}_2\text{O}) = 1.4 \times 10^{-4}$ and $r_m = \chi(\text{CH}_3\text{OH})/\chi(\text{H}_2\text{O}) = 1.4 \times 10^{-2}$. Although q_m and r_m constitute free parameters, we have fixed their values for comparison purposes with the L1448-mm outflow (Secs. 5 and 6).

3.2. Sputtering of the Grain Cores

For the sputtering of the cores, we have used different approaches to calculate the sputtering produced by collisions with H₂, and by collisions with He, C, O, Si, Fe and CO. We assume that olivine (MgFeSiO₄) is the main form of silicates in the cores. In the case of H₂, we calculate the angle-averaged sputtering yield as in Sec. 3.1 (see Eq. B.2 in the Appendix B), but considering a surface binding energy $U_0 = 5.70 \text{ eV}$ for the silicate cores (Tielens et al. 1994). For the sputtering agents He, C, O, Si and Fe, we have used the sputtering yields for olivine calculated by May et al. (2000, see Eq. B.3). Since CO has the same projectile mass as Si, we assume that the sputtering yield of CO is similar to that of Si (Field et al. 1997; May et al. 2000). The sputtering threshold energies E_{th} used for the projectiles are 73 eV for He, 48 eV for C, and 47 eV for O, Si, Fe and CO (Table 4 of May et al. 2000). To take into account the projection effects in the production of silicon within the shock, we have included the factor $1/\cos^2\theta$ in the impact energy E_p of the colliding particle (Eq. B.3), where θ is the inclination angle of the outflow with respect to the line of sight. For the L1448-mm outflow (see Secs. 5 and 6), θ is $\sim 70^\circ$ (Girart & Acord 2001). As for the mantles, the total sputtering rate for silicon is determined by Eq. (B.6), and (Eq. B.9) calculates the volume density of silicon ejected from the grain cores. In the case of H₂, we also need to consider that the probability for a silicon atom to be injected into the gas phase from an olivine molecule, as opposed to a Mg, Fe or O atom, q_c , is 0.2 (Caselli et al. 1997). However, for the rest of the colliding particles, we assume that $q_c = 1$ since this probability has been already taken into account in the calculations of the sputtering yields of May et al. (2000). Practically all silicon ($\sim 99.97\%$) is locked into the grain cores with an abundance of $\sim 3.6 \times 10^{-5}$ (see Table 2; Anders & Grevesse 1989; Snow & Witt 1996).

Table 3. Input parameters for the C-shock profiles shown in Figs. 1 and 2.

v_s (km s ⁻¹)	$n(H_2)$ (cm ⁻³)	B_0 (mG)	χ_e	z_n (cm)	z_i (cm)	z_T (cm)	z_0 (cm)	a_T (K ^{1/6} cm ⁻¹)	Δ (cm)	$T_{n,max}$ (K)
40	10 ⁴	0.14	7×10 ⁻⁸	7.0×10 ¹⁵	1.0×10 ¹⁵	1.8×10 ¹⁵	8.0×10 ¹⁵	9.0×10 ⁻¹⁶	5×10 ¹⁶	2000
35	10 ⁸	14	7×10 ⁻¹⁰	6.0×10 ¹³	2.0×10 ¹³	1.3×10 ¹³	0.0	1.3×10 ⁻¹³	2×10 ¹⁴	1700

**Fig. 1.** Comparison between our approximation of v_n , v_i , Δv , T_n and T_i (lower panels), and the MHD shock structure calculated as in Flower & Pineau des Forêts (2003, upper panels) for a shock with $v_s=40$ km s⁻¹, $n_0=10^4$ cm⁻³ and $B_0 = 100\mu G$ (Flower, private communication). Shock parameters are given in Table 3 and velocities are in the shock frame (see Appendix A for the definition of v_n and v_i).

4. Results

4.1. Validation of the Approximation of the Physical Structure of the C-shock

To validate the parametric approximation of the C-shock physical structure of Sec. 2, in Fig. 1 we show the comparison between the C-shock profile calculated as in the recent MHD models of Flower & Pineau des Forêts (2003), and the profiles of v_n , v_i , Δv , T_n and T_i derived in the shock frame through our approach (see Appendix A for details). In Fig. 2, we directly compare our results with the MHD shock structure obtained by Kaufman & Neufeld (1996). The values of z_n , z_i , z_T , z_0 and a_T chosen to reproduce these shock profiles (see below for the estimation of the input parameters), and the values of the magnetic field, B_0 , fractional ionization, χ_e , shock length scale, Δ , and

maximum temperature of the neutral fluid, $T_{n,max}$, are shown in Table 3.

From Fig. 1, it is clear that, although some differences do exist between the approximation and the MHD shock modelling at moderate preshock densities (Flower, private communication), the general behaviour of v_n , v_i , Δv , T_n and T_i , qualitatively mimics the physical structure of C-shocks. In particular, the velocity decoupling between the ion and neutral fluids in the magnetic precursor, and the initial *delay* in the switch on of the neutral heating at this stage, are well reproduced by our approximation. Note that the agreement between the profiles of v_n and v_i is excellent, giving a reliable prediction of Δv which is a key parameter in the sputtering yield calculation (see Appendix B). In order to fit the delay of the heating of the neutrals at the magnetic precursor stage, we need to impose $b_T \geq 6$.

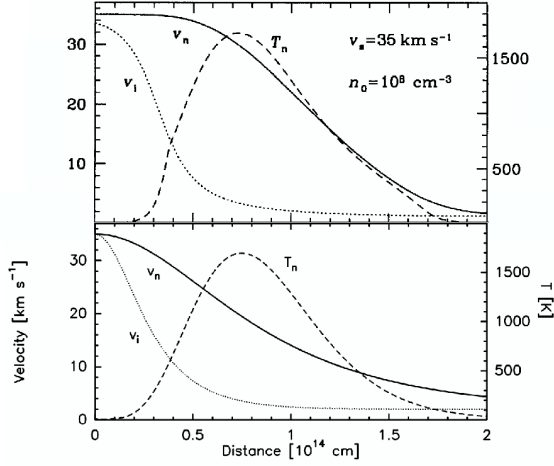


Fig. 2. Comparison between the profiles of v_n , v_i and T_n derived with our approximation (lower panel) and the MHD shock structure obtained by Kaufman & Neufeld (1996) for a shock with $v_s=35 \text{ km s}^{-1}$ and $n_0=10^8 \text{ cm}^{-3}$ (upper panel). Parameters are given in Table 3 and velocities are in the shock frame.

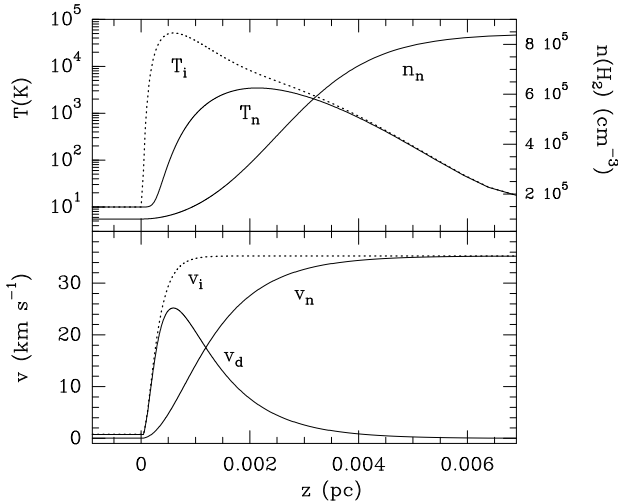


Fig. 3. C-shock physical structure obtained with Eqs. (1), (3) and (4) for $v_s = 40 \text{ km s}^{-1}$, $n_0 = 10^5 \text{ cm}^{-3}$ and $T_0 = 10 \text{ K}$. Velocities are in the frame co-moving with the preshock gas. The magnetic precursor length is of $\Delta z \sim 0.0005\text{--}0.001 \text{ pc} \sim 1.5\text{--}3.0 \times 10^{15} \text{ cm}$.

For higher preshock densities, Fig. 2 shows that the ion-neutral velocity decoupling in the magnetic precursor, is not as accurately reproduced as in Fig. 1 for the moderate density case (Flower & Pineau des Forêts 2003). We should mention, however, that the MHD treatment of C-shocks for high density regions, is still rather simplistic and therefore, uncertain (see Pilipp et al. 1990; Pilipp & Hartquist 1994; Falle 2003; Chapman & Wardle 2006). Since the existing perpendicular shock models may not start having problems until the preshock density exceeds 10^6 cm^{-3} (see e.g. Pilipp et al. 1990), in the following we will restrict our study to the moderate density case (from 10^4 to 10^6 cm^{-3}).

In Table 4, we summarize the different values of z_n , z_i , z_T and a_T , chosen to reproduce the physical structure of a sample of C-shocks with velocities of $10 \leq v_s \leq 40 \text{ km s}^{-1}$ and initial H_2 densities of $10^4 \leq n_0 \leq 10^6 \text{ cm}^{-3}$. z_n and z_i have been estimated by considering that v_n is $0.999 v_s$ at Δ , and by assuming a z_n/z_i ratio of $\sim 9/2$. We note that slightly higher (factor of 1.5) z_n/z_i ratios are required to reproduce the results of Flower & Pineau des Forêts (2003) with a new treatment of the coupling between the neutral and the charged fluids (Flower, private communication). However, for consistency, we will hereafter use the z_n/z_i ratio of $\sim 9/2$, since it well reproduces the results of Flower et al. (1996) and Draine et al. (1983), for which Dopita & Sutherland (2003) accordingly give an estimate of the shock length scale, Δ . In any case, the results obtained with both values of z_n/z_i do not differ by more than 15%.

The parameters a_T and z_T have been derived by assuming that $b_T=6$ and $z_0=0 \text{ cm}$. The magnetic field, B_0 , and fractional ionization of the gas, χ_e , have been calculated as in Draine et al. (1983), and the shock length scale, Δ , as in Dopita & Sutherland (2003). The estimated Alfvén velocity is of $v_A=2.18 \text{ km s}^{-1}$, and v_0 typically ranges from 3.1 to 4.7 km s^{-1} for the cases considered in Table 4 (see Appendix A for the calculation of v_A and v_0). We note that the shock length scales derived for every initial H_2 density of Table 4, are of the same order of magnitude as the ion-neutral coupling lengths determined by Kaufman & Neufeld (1996, see Fig. 1 in this work). The maximum temperature of the neutral fluid, $T_{n,max}$, has been estimated from the results of Draine et al. (1983).

In Fig. 3, we show a representative profile of a C-shock with $v_s=40 \text{ km s}^{-1}$, $n_0=10^5 \text{ cm}^{-3}$ and $T_0=10 \text{ K}$. As expected in the frame co-moving with the preshock gas, the ion and neutral fluids are at rest at the beginning of the shock, and their final velocities in the far downstream gas are of $\sim v_s - v_0$ (see Draine et al. 1983). The initial delay of the heating of the neutrals gives the magnetic precursor length, which is of $\Delta z \sim 0.0005\text{--}0.001 \text{ pc} \sim 1.5\text{--}3.0 \times 10^{15} \text{ cm}$ (Fig. 3). While the maximum value of the temperature of the ions is correlated with the maximum value of v_d (see Fig. 3), the neutrals show their maximum temperature at $v_n \sim 0.85 v_s$ (derived by assuming H_2O cooling and $\alpha_c=1.5$ in Eq. 18 of Smith & Brand 1990), which is consistent with the results of Kaufman & Neufeld (1996, see Fig. 2).

From the recent results of time-dependent shock modelling, one may consider that our assumption of steadiness for the C-shock could not be valid to describe the time evolution of the sputtering of grains. These models indeed show that a J-type component is a natural feature in the far downstream gas of the C-shock (near the *piston*) for time-scales of $\leq 10^3\text{--}10^4 \text{ yr}$, for which the steady state is finally attained (Chièze et al. 1998; Lesaffre et al. 2004). However, as shown in Sec. 4.2, the evolutionary stages relevant to the main injection of the material contained in the icy mantles and in the grain cores are those of the magnetic precursor which, independently on the age of the shock, can be described by the steady state profile of C-shocks (Chièze et al. 1998; Lesaffre et al. 2004).

Table 4. Input parameters for a sample of C-shocks.

v_s (km s ⁻¹)	v_0^a (km s ⁻¹)	$n(H_2)$ (cm ⁻³)	B_0^b (μG)	χ_e^b	z_n (cm)	z_i (cm)	z_T^c (cm)	a_T^c (K ^{1/6} cm ⁻¹)	Δ^d (pc)	$T_{n,max}^e$ (K)
20	3.8	10 ⁴	140	7×10 ⁻⁸	1.4×10 ¹⁶	3.2×10 ¹⁵	5.0×10 ¹⁵	2.9×10 ⁻¹⁶	0.024	900
40	4.7	10 ⁴	140	7×10 ⁻⁸	2.8×10 ¹⁶	6.2×10 ¹⁵	1.1×10 ¹⁶	1.5×10 ⁻¹⁶	0.048	2200
10	3.1	10 ⁵	450	2×10 ⁻⁸	7.7×10 ¹⁴	1.7×10 ¹⁴	2.0×10 ¹⁴	5.8×10 ⁻¹⁵	0.0012	300
20	3.8	10 ⁵	450	2×10 ⁻⁸	1.4×10 ¹⁵	3.2×10 ¹⁴	5.0×10 ¹⁴	2.8×10 ⁻¹⁵	0.0024	800
30	4.3	10 ⁵	450	2×10 ⁻⁸	2.1×10 ¹⁵	4.7×10 ¹⁴	8.0×10 ¹⁴	2.0×10 ⁻¹⁵	0.0036	2000
40	4.7	10 ⁵	450	2×10 ⁻⁸	2.8×10 ¹⁵	6.2×10 ¹⁴	1.1×10 ¹⁵	1.6×10 ⁻¹⁵	0.0048	4000
20	3.8	10 ⁶	1400	7×10 ⁻⁹	1.4×10 ¹⁴	3.2×10 ¹³	5.0×10 ¹³	2.8×10 ⁻¹⁴	2.4×10 ⁻⁴	800
40	4.7	10 ⁶	1400	7×10 ⁻⁹	2.8×10 ¹⁴	6.2×10 ¹³	1.1×10 ¹⁴	1.6×10 ⁻¹⁴	4.8×10 ⁻⁴	4000

^a Calculated with Eq. A.4 (see Appendix A) and assuming $v_A=2.18$ km s⁻¹.

^b Estimated using Eqs. (62) and (63) of Draine et al. (1983).

^c Calculated considering that $b_T=6$ and $z_0=0$ cm.

^d Derived as in Dopita & Sutherland (2003) and assuming that $n_{0,i}/n_H \sim 10^{-6}$.

^e Taken from Figs. 8b and 9b of Draine et al. (1983) for $n_0=10^4$ cm⁻³, and $n_0=10^5$ and 10^6 cm⁻³ respectively.

4.2. Sputtered Silicon Abundances: Injection and Saturation Times.

We now include the evolutionary profiles of v_n , v_i , T_n , T_i and n_n from Sec. 4.1 in the sputtering equations of the Appendix B to calculate the silicon abundances ejected from the mantles and from the cores. Fig. 4 shows the silicon abundances ejected from grains as a function of the flow time for several H₂ gas densities and shock velocities. The abundances of sputtered silicon do not practically change with the initial density of the gas, which is clearly in agreement with the results of Caselli et al. (1997). However, as expected from the strong dependence of the sputtering rate on the maximum value of v_d (see Eq. B.1 and Pineau des Forêts et al. 1997), the silicon abundance is drastically enhanced by increasing shock velocities. From Fig. 4, we also note that the time-scales are progressively reduced by nearly a factor of 10 as we increase the H₂ density from 10⁴ to 10⁵ and 10⁶ cm⁻³. This is consistent with the fact that the flow time, t , is inversely proportional to the density (the cooling time-scales roughly vary as n_i^{-1} , where n_i is proportional to the density; see Chièze et al. 1998; Lesaffre et al. 2004).

In Fig. 5, we show the products of the sputtering of the mantles and of the cores for an initial density of 10⁵ cm⁻³ and for shock velocities of 10, 20, 30 and 40 km s⁻¹. The sputtering of the grain mantles by collisions with H₂ and He (in bold lines in Fig. 5) exactly corresponds to that previously calculated by Caselli et al. (1997). Although the fractional abundance of the heavy species is orders of magnitude smaller than that of H₂ and He (see Sec. 3.1), it is clear that the heavy atoms and CO sputter the mantles much more efficiently than H₂ or He for low shock velocities (Fig. 5).

The high efficiency of these heavy species as sputtering agents is also shown by the *injection*, t_{inj} , and *saturation* times, t_{sat} , of Table 5. We define t_{inj} as the time for which the gas phase silicon abundance, relative to H₂, exceeds 10⁻²⁰ (i.e. the lower limit of Fig. 5); and t_{sat} as the time for which the difference (in the logarithmic scale) of the silicon abundance between two consecutive time steps t_{i+1} and t_i (see Appendix A) is $|\log_{10}[\chi(m)]_{i+1} - \log_{10}[\chi(m)]_i| < 0.1$. Table 5 also shows the

injection and saturation times due to the contribution of all colliding particles. We note that these times are a factor of ~ 100 smaller than the typical dynamical ages of young molecular outflows like L1448-mm (~ 1000 yr), but are roughly of the same order of magnitude as the time-scales derived for the young shocks found in this outflow (≤ 90 yr; Girart & Acord 2001). From Table 5, we find that the injection and saturation times of H₂ and He are larger than those of the heavy atoms and of CO.

For the heavy colliding particles, CO seems to dominate the sputtering of the icy water mantles in low velocity shocks. Although Fe initiates the grain sputtering (Fe has the smallest injection and saturation times; see Table 5), its low fractional abundance prevents large enhancements of silicon by the impact with this element ($\leq 3 \times 10^{-14}$ for $v_s \leq 20$ km s⁻¹; Fig. 5). On the contrary, collisions with CO (whose injection and saturation times are very similar to those of Si but whose initial abundance is 4 orders of magnitude larger than that of Si) produce the main injection of silicon from the mantles. The saturation times for CO are indeed very similar to those derived for all colliding particles at low shock velocities (see Table 5).

The abundance of silicon sputtered by collisions with CO for $v_s \leq 10$ km s⁻¹ is very low ($\sim 10^{-12}$; Fig. 5). However, at slightly higher shock velocities ($v_s = 20$ km s⁻¹), this abundant molecule can eject from the mantles considerable amounts of this element ($\sim 10^{-9}$). Averaging this silicon abundance over the dissipation region (shock length scale of $\sim 7 \times 10^{15}$ cm; see Tab. 4), we estimate that the total column density of silicon injected into the gas phase in a 20 km s⁻¹-shock is of $\sim 10^{12}$ cm⁻². While shock velocities of $v_s \geq 25$ km s⁻¹ were required to obtain Si/SiO column densities of $\geq 10^{12}$ cm⁻² in May et al. (2000), we find that the inclusion of silicon as a minor constituent of the grain mantles reduces the sputtering *threshold velocity* by, at least, $|\sim 5$ km s⁻¹| in our model with respect to previous results. This velocity threshold is even reduced by $|\sim 10$ km s⁻¹| compared to the results of Caselli et al. (1997).

It is also interesting to note that CO can also generate silicon abundances of $\sim 2 \times 10^{-11}$ at the very early stages of low velocity shocks ($t \leq 10$ yr; see cases with $v_s=20$ and 30 km s⁻¹

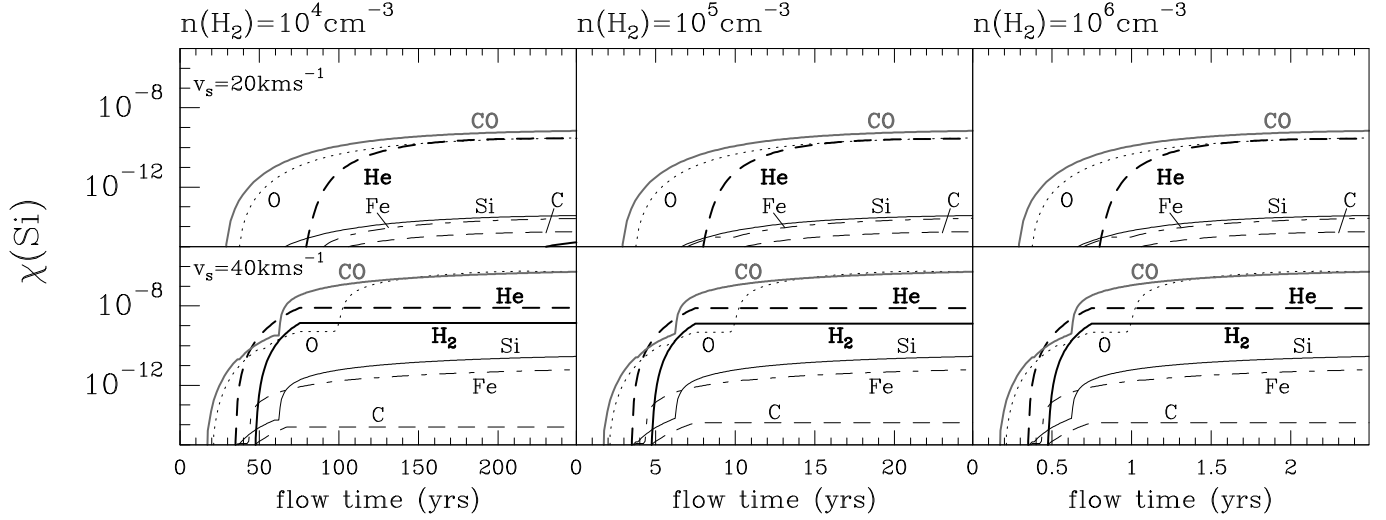


Fig. 4. Evolution of the abundance of elemental silicon ejected from grains by the impact with H_2 , He, C, O, Si, Fe and CO, for initial H_2 densities of 10^4 , 10^5 and 10^6 cm^{-3} and shock velocities of 20 and 40 km s^{-1} .

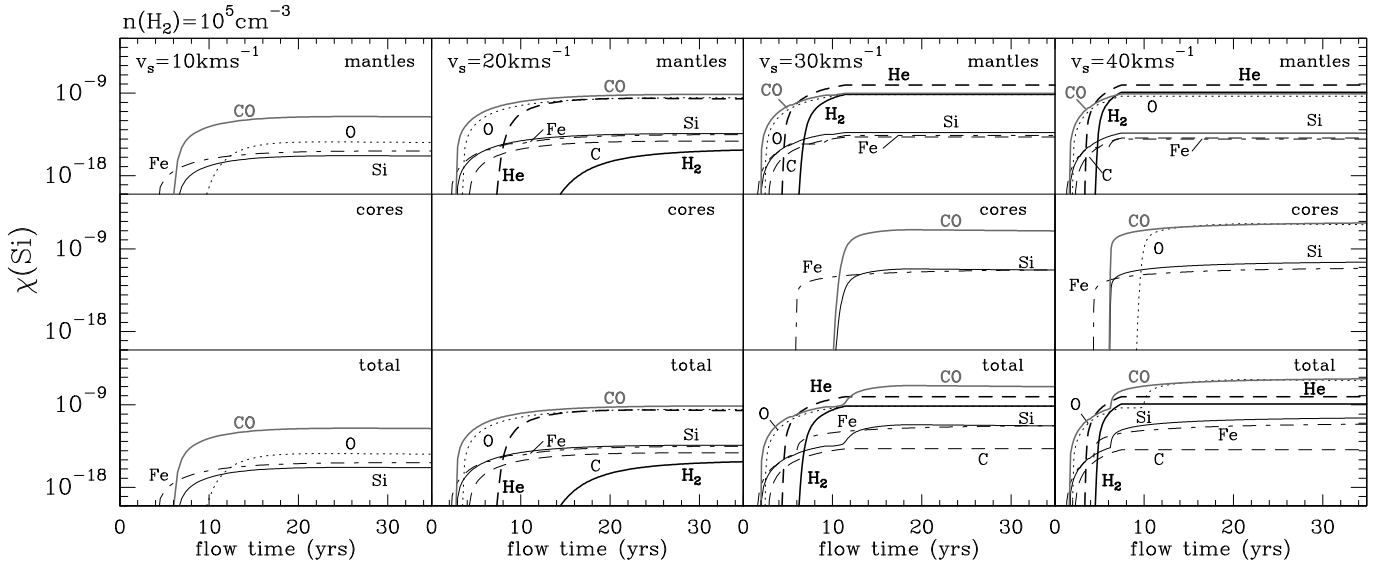


Fig. 5. Abundance of elemental silicon ejected from grains by the impact with H_2 , He, C, O, Si, Fe and CO, for shock velocities of 10, 20, 30 and 40 km s^{-1} and a H_2 gas density of 10^5 cm^{-3} . For each shock velocity, we show the individual production of silicon from the mantles (upper panels), from the cores (middle panels), and the total production of silicon from grains (lower panels).

in Fig. 5). As discussed in Sec. 5, these results could explain the detection of SiO abundances of $\sim 10^{-11}$ associated with the narrow SiO emission observed in the young shocks of the L1448-mm outflow.

For shocks with $v_s \geq 30 \text{ km s}^{-1}$, He plays an important role in the sputtering of the mantles. Note that the saturation times for all colliding particles at these shock velocities, slightly deviate from those of CO due to the increasing efficiency of He to erode the grain mantles (Table 5 and Fig. 5). Almost all silicon within the mantles ($\sim 8 \times 10^{-9}$) is injected into the gas phase by collisions with He for shock velocities of $v_s \sim 30 \text{ km s}^{-1}$.

For the sputtering of the grain cores, only collisions with O, Si, Fe and CO are efficient enough to destroy the cores. The injection of silicon into the gas phase from the cores occurs for

shock velocities $v_s \geq 30 \text{ km s}^{-1}$, which is consistent with the results of May et al. (2000). For $v_s = 40 \text{ km s}^{-1}$, only $\sim 3\%$ of the total amount of silicon locked into the grain cores, is released into the gas phase (abundance of $\sim 10^{-6}$; see Fig. 5). As for the mantles, and although Si has the same injection and saturation times as those of CO (both are assumed to have similar sputtering properties for the cores; see Sec. 3.2), CO is the main sputtering agent of the grain cores since its initial fractional abundance clearly exceeds that of Si.

5. Comparison with Observations: The SiO Abundances

If we now assume that silicon is rapidly oxidized into SiO (Pineau des Forêts et al. 1997) or that SiO is directly released

Table 5. Injection and saturation times for the grain mantles and the grain cores for a medium with an initial H_2 density of $n_0 = 10^5 \text{ cm}^{-3}$.

	Mantles								Cores							
	$v_s \text{ (km s}^{-1}\text{)}$								$v_s \text{ (km s}^{-1}\text{)}$							
	10		20		30		40		10		20		30		40	
	Inj.	Sat.	Inj.	Sat.	Inj.	Sat.	Inj.	Sat.	Inj.	Sat.	Inj.	Sat.	Inj.	Sat.	Inj.	Sat.
H_2	14.6	16.3	6.3	8.2	4.6	6.0
He	7.4	10.1	4.4	6.3	3.4	5.0
C	4.4	6.4	2.9	4.9	2.3	4.1
O	9.8	14.4	3.7	6.0	2.5	4.7	2.1	3.9	9.2	10.4
Si	6.9	10.5	2.9	5.7	2.1	4.3	1.8	3.6	10.5	11.9	6.2	6.6
Fe	4.5	8.6	2.3	5.1	1.8	3.5	1.3	2.6	5.9	6.5	4.3	4.8
CO	6.5	10.5	2.9	5.7	2.1	4.3	1.8	3.6	10.2	11.9	6.1	6.6
all	4.5	10.5	2.3	5.7	1.8	4.4	1.3	4.6	5.9	11.9	4.3	6.6

NOTE. — The injection and saturation times are given in yr.

from grains (Martín-Pintado et al. 1992), we can directly compare our predictions of the silicon abundance ejected from grains by the sputtering, with the SiO abundances observed in very young bipolar outflows like in L1448-mm.

In Fig. 6, we show the SiO abundances measured for the different velocity components detected in this outflow (ambient gas, the shock precursor component, the moderate velocity gas and the high velocity gas; Jiménez-Serra et al. 2005; Martín-Pintado et al. 1992) as a function of the flow time. For the ambient and precursor components, we have assumed central radial velocities of $v_{LSR} = 4.7$ and 5.2 km s^{-1} , respectively (Jiménez-Serra et al. 2004). Subtracting the ambient cloud velocity of $v_{cl} = 4.7 \text{ km s}^{-1}$ characteristic of the molecular emission in L1448-mm from the central radial velocities of these components (see Eq. 5 in Sec. 2), we obtain flow velocities of $v_n = 0$ and 0.5 km s^{-1} , which correspond to flow times of $t=0$ and 4.0 yrs for the ambient gas and the precursor component in a 30 km s^{-1} -shock (Eq. 2 of Sec. 2; see also Eq. A.7 in Appendix A for the details on the computation of the flow times). For the moderate velocity gas, we have considered velocity intervals of 1 km s^{-1} -width between 6 and 18 km s^{-1} (Jiménez-Serra et al. 2005). The SiO abundances for the ambient, precursor and moderate velocity gas have been derived assuming optically thin emission and excitation temperatures of $\sim 10\text{--}15 \text{ K}$ (Requena-Torres et al. 2007). For the high velocity gas, the SiO abundances of $\sim 10^{-6}$ and 2×10^{-6} (Fig. 6) have been taken from Tab. 6 in Martín-Pintado et al. (1992) for the velocity ranges of $-50 \text{ km s}^{-1} \leq v_{LSR} \leq -40 \text{ km s}^{-1}$ and $-60 \text{ km s}^{-1} \leq v_{LSR} \leq -50 \text{ km s}^{-1}$. The flow time associated with each velocity interval is again estimated from their central radial velocities, v_{LSR} , after subtracting the ambient cloud velocity of the L1448-mm outflow of $v_{cl} = 4.7 \text{ km s}^{-1}$ (Eq. 5).

Fig. 6 also shows the silicon abundances, as a function of time, predicted by our model for the shocks which best fit the observational SiO data (with $v_s = 30 \text{ km s}^{-1}$ and $v_s = 60 \text{ km s}^{-1}$). The shock parameters used to reproduce the physical structure of these shocks are shown in Table 6.

From Fig. 6, we note that the sputtering produced by the propagation of a 30 km s^{-1} -shock perfectly matches the evolutionary trend of SiO to be enhanced from the ambi-

ent to the moderate velocity gas observed in L1448-mm (Jiménez-Serra et al. 2005). The progressive erosion of the icy mantles by the sputtering with CO, reproduces the SiO abundances observed in the ambient gas ($\leq 10^{-12}$; filled square), in the precursor component ($\sim 10^{-11}$; filled circle), and in the moderate velocity gas (from $\sim 10^{-9}$ to $\sim 10^{-8}$; filled triangles in Fig. 6). This suggests that the puzzling narrow SiO line detected toward the young shocks of L1448-mm can be explained by the recent erosion of the grain mantles containing a small fraction of Si/SiO, at the early stages of low velocity shocks.

To fit the SiO abundances measured in the high velocity gas, a velocity shock with $v_s = 60 \text{ km s}^{-1}$ is needed to sputter $\sim 9\%$ of the silicon contained within the olivine cores and increase the predicted silicon abundance up to a few 10^{-6} (filled stars in Fig. 6). This shock velocity is clearly in excess of the critical velocities of C-shocks ($v_{crit} \sim 40\text{--}50 \text{ km s}^{-1}$; see Draine et al. 1983; Smith & Brand 1990). Le Bourlot et al. (2002) and Cabrit et al. (2004) have recently shown that the actual shock velocity limit can be increased to $v_{crit} \sim 100 \text{ km s}^{-1}$ for moderate densities and high magnetic fields. However, we cannot rule out the possibility that a J-type component would be the responsible for the large SiO abundances observed in the high velocity gas of L1448-mm.

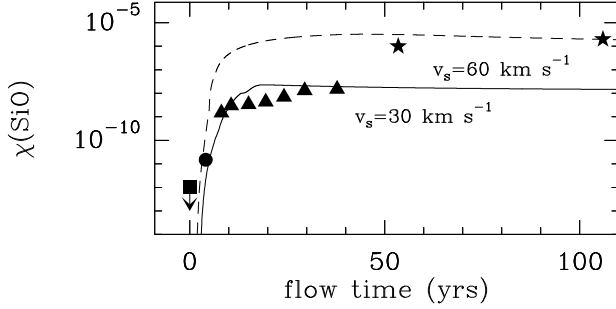
Given the fact that the L1448-mm outflow shows variability in its high velocity SiO emission, an alternative scenario would involve the presence of two different shocks at two different evolutionary stages that would coexist within the single-dish beam of the SiO observations (Jiménez-Serra et al. 2005).

6. Sputtered CH_3OH and H_2O Abundances.

In addition to SiO, CH_3OH and H_2O are also expected to be largely enhanced in outflow regions (see e.g. Draine et al. 1983; Kaufman & Neufeld 1996). In Fig. 7 (upper and middle panels), we show the predicted abundances of CH_3OH and H_2O as a function of the flow time, for a sample of shocks with $v_s = 10, 20, 30$ and 40 km s^{-1} (see Table 4). The impact with CO injects CH_3OH and H_2O abundances as large as $\sim 10^{-7}$ and $\sim 10^{-5}$, respectively, in low velocity shocks (see cases with $v_s = 20 \text{ km s}^{-1}$; Fig. 7). These abundances are even enhanced to

Table 6. Parameters of the C-shock models that best fit the SiO and CH₃OH observational data shown in Figs. 6 and 7.

v_s (km s ⁻¹)	$n(\text{H}_2)$ (cm ⁻³)	B_0 (μG)	Δ (pc)	$T_{n,\text{max}}$ (K)	z_n (cm)	z_i (cm)	z_T (cm)	a_T (K ^{1/6} cm ⁻¹)	z_n/z_i
30	10 ⁵	450	0.0036	2000	2.1×10^{15}	5.0×10^{14}	8.0×10^{14}	2.0×10^{-15}	4.2
60	10 ⁵	450	0.0072	6000	4.1×10^{15}	1.0×10^{15}	1.1×10^{15}	1.8×10^{-15}	4.0

**Fig. 6.** Predicted SiO abundances within a 30 km s⁻¹- and a 60 km s⁻¹-shock as a function of the flow time (see shock parameters in Table 6). Observational SiO abundances derived in the ambient gas (filled square), the precursor component (filled circle), the moderate velocity gas (filled triangles) and the high velocity regime (filled stars) found in the L1448-mm outflow (Martín-Pintado et al. 1992; Jiménez-Serra et al. 2005), are also shown. The black arrow indicates an upper limit to the SiO abundance. The observed flow times have been derived from Eq. 2 of Sec. 2 (see text and Appendix A for details).

up to $\sim 10^{-6}$ for CH₃OH, and to $\sim 10^{-4}$ for H₂O, in shocks with only $v_s = 30$ km s⁻¹.

We can now compare the predicted abundances of CH₃OH and H₂O with those observed in the young shocks of the L1448-mm outflow. Fig. 7 (lower panel) shows the SiO and CH₃OH abundances observed in the ambient gas (square), the precursor component (circles) and the moderate velocity gas (triangles) of this outflow (Jiménez-Serra et al. 2005), as a function of the flow time. In this figure, we also show the abundances of ortho-H₂O derived from the line profile of the 1₁₀→1₀₁ transition measured by SWAS (Benedettini et al. 2002). Since the velocity resolution of these observations (~ 1 km s⁻¹; Benedettini et al. 2002) is lower than those of the SiO and CH₃OH spectra (~ 0.14 km s⁻¹; see Jiménez-Serra et al. 2005), we have only estimated the abundances of ortho-H₂O for the moderate velocity regime (dark grey triangles in Fig. 7). As in Sec. 5, the flow times associated with these abundances have been inferred subtracting the ambient cloud velocity in L1448-mm of $v_{cl} = 4.7$ km s⁻¹ from the central velocities, v_{LSR} , of the observed line profiles of these molecules (see Eq. 5). The SiO, CH₃OH and H₂O abundances have been derived assuming optically thin emission as in Jiménez-Serra et al. (2005) for SiO and CH₃OH, and as in Neufeld et al. (2000) for H₂O (Eq. 1 in this work). The abundance of SiO (black line), CH₃OH (light grey line) and H₂O (dark grey line) in gas phase generated by the sputtering of the grain mantles in the 30 km s⁻¹-shock of Sec. 5 (see Table 6) are also shown in Fig. 7.

As for SiO, the abundance of sputtered CH₃OH is in agreement with that derived in the precursor component within one order of magnitude, and with those measured in the moderate velocity gas within a factor of ≤ 5 (see Fig. 7). We would like to stress that we have only argued the total amount of material in the grain mantles. This implies that the progressive enhancement of the SiO and CH₃OH abundances observed for velocities of ≤ 20 km s⁻¹ toward L1448-mm (Jiménez-Serra et al. 2005), is naturally explained by the presence of a single shock with $v_s = 30$ km s⁻¹. In the case of ortho-H₂O, however, the abundances of this molecule in the moderate velocity gas differ by more than a factor of 10 from those predicted by our model. This could be due either to the assumption of optically thin emission for the ortho-H₂O 1₁₀→1₀₁ transition (which could have underestimated the ortho-H₂O abundances; Benedettini et al. 2002), or to a beam dilution effect. Note that the SWAS beam is of $\sim 240''$, i.e., 8 times larger than the 30 m beam of the SiO $J=2 \rightarrow 1$ observations (Jiménez-Serra et al. 2005). This leads to a *corrected* ortho-H₂O abundance of some $\sim 10^{-4}$, which is consistent with our model predictions of Fig. 7.

7. Conclusions

In this work, we have presented a parametric model that mimics the steady state profile of the physical parameters of C-shocks. The simplicity of this model has allowed, for the first time, the detailed analysis of the time evolution of the sputtering of the grain mantles and the grain cores in regions with recent outflow activity. Although this approximation does not include detailed MHD modelling, we have shown that it can be used as an efficient tool to interpret the time dependent evolution of the abundances of typical shock tracers like SiO, CH₃OH, H₂O or NH₃ in young molecular outflows, where transient phenomena are expected to play an important role. The assumption of steadiness of the shock can be applied for these young objects, since only the early stages of the shock evolution (characterized exclusively by the interaction of the magnetic precursor) are relevant for the process of the sputtering of dust grains.

To calculate the sputtering of the grain mantles and the grain cores, we have assumed that silicon and methanol are minor constituents of the water mantles, and that olivine is the main form of silicates within the grain cores. In spite of the low fractional abundance of heavy atoms (C, O, Si and Fe) and molecules (CO) relative to H₂ or He in molecular dark clouds, these species have been also considered as sputtering agents. The relatively high abundance of CO with respect to the rest of heavy colliding particles, and its large sputtering yield, makes the sputtering by CO very efficient. Collisions with this molecule can eject a considerably large fraction of silicon in the mantles for shocks with only $v_s \sim 20$ km s⁻¹. This implies

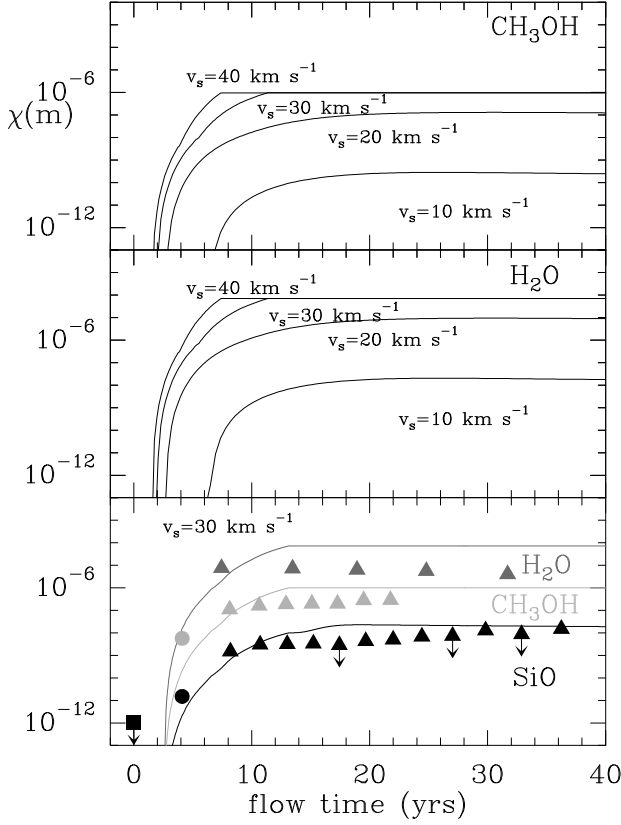


Fig. 7. *Upper and middle panels:* Predictions of the sputtered abundances of CH_3OH and H_2O as a function of the flow time, for a sample of C-shocks with $v_s = 10, 20, 30$ and 40 km s^{-1} and $n_0 = 10^5 \text{ cm}^{-3}$. *Lower panel:* SiO , CH_3OH and H_2O abundances ejected from the grain mantles for the 30 km s^{-1} -shock of Table 6 as a function of time. We also show the SiO , CH_3OH and H_2O abundances measured in the ambient gas (square), the precursor component (circles) and the moderate velocity gas (triangles) of the L1448-mm outflow (Jiménez-Serra et al. 2005; Benedettini et al. 2002). Vertical arrows indicate upper limits to the SiO abundance.

a reduction by $\sim 5\text{--}10 \text{ km s}^{-1}$ of the *threshold velocity* of the sputtering with respect to other models.

By comparing the evolution of the abundances of SiO , CH_3OH and H_2O predicted by our model, with the abundances derived toward the different velocity regimes found in the young shocks of the L1448-mm outflow, we find that two different shocks (with $v_s = 30 \text{ km s}^{-1}$ and $v_s = 60 \text{ km s}^{-1}$) are needed to reproduce the measured abundances. The progressive enhancement of SiO and CH_3OH observed from the ambient gas up to moderate velocities, is consistent with the mantle erosion produced by a single 30 km s^{-1} -shock. We find that the SiO abundance of $\sim 10^{-11}$ associated with the very narrow SiO emission detected in this outflow, can be explained as an early product of the sputtering of the mantles by CO in low velocity shocks if the Si/SiO abundance in the grain mantles is $\sim 10^{-4}$ with respect to water. The disagreement between the predicted and the derived ortho- H_2O abundances is probably due either to the assumption of optically thin emission for the ortho- H_2O $1_{10} \rightarrow 1_{01}$ line observed by SWAS, or to a beam dilution effect.

The approximation presented in this work, not only will furnish an input for more comprehensive MHD models of the shock structure in young molecular outflows, but will allow to perform direct comparisons with the molecular line profiles observed toward these regions. These comparisons will be presented in a future paper.

Acknowledgements. We are indebted to Prof. D. R. Flower for his comments on the C-shock and sputtering theory and for kindly providing the MHD shock structure shown in Fig. 1. We acknowledge Dr. M. Kaufman for letting us use his MHD shock profile shown in Fig. 2. We would like to thank Dr. A. Asensio-Ramos for the help provided during the development of the code, and Dr. F. Daniel for his useful comments on the manuscript. We also acknowledge an anonymous referee for helping us to significantly improve the paper. This work was supported by the Spanish MEC through projects number AYA2003-02785-E, ESP2004-00665 and ESP2007-65812-C02-01, and by the “Comunidad de Madrid” Government under PRICIT project S-0505/ESP-0277 (ASTROCAM). PC acknowledges support from the Italian Ministry of Research and University within a PRIN project.

Appendix A: The C-shock Structure in the Shock Frame

The steady-state velocity profiles of the ion and neutral fluids, v_i^* and v_n^* , within the frame of the shock, are approximated as:

$$v_{n,i}^* = v_0 + \frac{(v_s - v_0)}{\cosh[(z - z_0)/z_{n,i}]} \quad (\text{A.1})$$

where z is the spatial coordinate and v_s is the velocity of the shock. z_0 , z_i and z_n are input parameters that govern the velocity decoupling between the ions and the neutrals (see Secs. 2 and 4.1), and v_0 is required to avoid infinite compression of the far downstream gas (see Eq. A.5 and Sec. 2). This speed only depends on the speed of the shock, v_s , and the Alfvén speed, v_A (see Eq. A.4 below). From Eq. A.1, it is clear that the ion and neutral fluids initially move with velocities v_s and are progressively decelerated to v_0 (see Figs. 1 and 2).

Assuming that the thermal pressure of the fluid is negligible compared to the magnetic and the dynamic pressures, we can estimate the magnitude of v_0 in the downstream gas from:

$$\rho_0 v_s^2 + \frac{B_0^2}{8\pi} = \rho v_0^2 + \frac{B^2}{8\pi} \quad (\text{A.2})$$

where ρ_0 and ρ are the preshock and postshock gas mass densities, and B_0 and B are the magnitude of the magnetic field in the preshock and postshock regimes, respectively. Considering that the compression of the magnetic field is given by $B = B_0(v_s/v_0)$ and that the Alfvén speed, v_A , is defined as $v_A^2 = B_0^2/(4\pi\rho)$, Eq. A.2 becomes:

$$v_0^2 = \frac{v_s^2}{\rho/\rho_0} + \frac{v_A^2}{2} \left[1 - \left(\frac{\rho}{\rho_0} \right)^2 \right] \quad (\text{A.3})$$

From the principle of mass conservation, the fluid density in the postshock gas, ρ , is derived as $\rho = \rho_0(v_s/v_0)$. If we now substitute the ratio ρ/ρ_0 in Eq. A.3, we finally obtain:

$$v_0^2 \left[v_0^2 - v_0 v_s - \frac{v_A^2}{2} \right] = -\frac{v_A^2}{2} v_s^2 \quad (\text{A.4})$$

from which v_0 can be calculated.

The particle density of the neutral fluid, n_n , is given by:

$$n_n = n_0 v_s / v_n^* \quad (\text{A.5})$$

and the time associated with the neutral fluid or flow time, t , in the frame of the shock is calculated as:

$$t = \int \frac{dz}{v_n^*} \quad (\text{A.6})$$

In each plane-parallel slab of material $i + 1$ within the shock, the flow time, t_{i+1} , is calculated by using the trapezoidal method:

$$t_{i+1} = t_i + (z_{i+1} - z_i) \left(\frac{f(z_i) + f(z_{i+1})}{2} \right) \quad (\text{A.7})$$

where z_i and z_{i+1} are the spatial coordinates for the slabs of gas i and $i + 1$, and $f(z_i)$ is defined as (see Eq. A.6):

$$f(z_i) = \frac{1}{v_n^*(z_i)} \quad (\text{A.8})$$

The temperature of the ion and neutral fluids, T_i and T_n , are estimated as in Sec. 2.

Appendix B: Sputtering of Grains. Silicon, CH₃OH and H₂O Fractional Abundances.

The sputtering of grains has been calculated by considering different sputtering yields for the mantles and for the cores. The sputtering rate per unit volume for a spherical target of radius a moving with drift velocity v_d through a Maxwellian neutral gas of temperature T_n is (Eq. 27 in Draine & Salpeter 1979):

$$\left[\frac{dn(m)}{dt} \right]_{\text{grain}} = \pi a^2 n_p \left(\frac{8kT_n}{\pi m_p} \right)^{1/2} \times \int_{x_{th}}^{\infty} dx x^2 \frac{1}{2} \left[e^{-(x-s)^2} - e^{-(x+s)^2} \right] < Y(E) >_{\theta} \quad (\text{B.1})$$

where n_p and m_p are the number density and mass of the projectile, respectively; and s and x are related to v_d , T_n and the projectile impact energy E_p through $s^2 = \frac{m_p v_d^2}{2kT_n}$ and $E_p = x^2 kT_n$.

The angle-averaged sputtering yield at low energies $< Y(E) >_{\theta}$ for the mantles can be approximated by

$Y(E) >_{\theta} \approx 2Y(E, \theta = 0)$ (Draine 1995), where the normal-incidence yield $Y(E, \theta = 0)$ is calculated as (Eq. 31; Draine & Salpeter 1979):

$$Y(E, \theta = 0) = A \frac{(\varepsilon - \varepsilon_0)^2}{1 + (\varepsilon/30)^{4/3}}, \quad \varepsilon > \varepsilon_0 \quad (\text{B.2})$$

A is a constant ($A \approx 8.3 \times 10^{-4}$), and ε and ε_0 are calculated as $\varepsilon = \eta E_p / U_0$ and $\varepsilon_0 = \max[1, 4\eta]$. U_0 is the binding energy (per atom or molecule) and η is derived by doing $\eta = 4\xi m_p M_t (m_p + M_t)^{-2}$, where M_t is the target mass and ξ is an efficiency factor which varies from 0.8 (for ices) to 1 (for atomic solids; Draine & Salpeter 1979). x_{th} , which is related to the threshold impact energy E_{th} , is finally calculated as $x_{th} = \left(\frac{\varepsilon_0 U_0}{\eta k T_n} \right)^{1/2}$.

For the grain cores, we have used the sputtering yield calculated by May et al. (2000) for the impact of atomic species on olivine cores. The sputtering yield is derived from:

$$< Y(E) >_{\theta} = k_s \exp \left[-\beta / (E_p - E_{th}) \right] \quad (\text{B.3})$$

where k_s , β and E_{th} (the sputtering threshold energy) are taken from Table 4 in May et al. (2000). In this case, x_{th} is derived by doing $x_{th} = \left(\frac{E_{th}}{k T_n} \right)^{1/2}$.

In each collision between projectile and grain, only a small fraction of silicon, q_m , and CH₃OH, r_m , will be ejected from the mantles [$q_m = 1.4 \times 10^{-4}$ and $r_m = 1.4 \times 10^{-2}$; see Sec. 3.1]. Analogously, only a fraction of silicon, q_c , will be released from the cores [$q_c = 0.2$ for H₂ and $q_c = 1$ for the rest of colliding particles; see Sec. 3.2]. If we assume a grain density n_g , the total sputtering rate for H₂O, CH₃OH and silicon is:

$$\left[\frac{dn(\text{H}_2\text{O})}{dt} \right]_{\text{tot}}^m = n_g \left[\frac{dn(\text{H}_2\text{O})}{dt} \right]_{\text{grain}}^m \quad (\text{B.4})$$

$$\left[\frac{dn(\text{CH}_3\text{OH})}{dt} \right]_{\text{tot}}^m = n_g r_m \left[\frac{dn(\text{CH}_3\text{OH})}{dt} \right]_{\text{grain}}^m \quad (\text{B.5})$$

$$\left[\frac{dn(\text{Si})}{dt} \right]_{\text{tot}}^{m,c} = n_g q_{m,c} \left[\frac{dn(\text{Si})}{dt} \right]_{\text{grain}}^{m,c} \quad (\text{B.6})$$

where m and c denotes the sputtering rate for the mantles and the cores.

By using the Euler's algorithm, we calculate the total volume density of H₂O, CH₃OH and Si ejected from grains in each plane-parallel slab of material i within the shock as:

$$n(\text{H}_2\text{O})_{i+1} = n(\text{H}_2\text{O})_i + \Delta t \left[\frac{dn(\text{H}_2\text{O})}{dt} \right]_{\text{tot},i}^m \quad (\text{B.7})$$

$$n(\text{CH}_3\text{OH})_{i+1} = n(\text{CH}_3\text{OH})_i + \Delta t \left[\frac{dn(\text{CH}_3\text{OH})}{dt} \right]_{\text{tot},i}^m \quad (\text{B.8})$$

$$n(\text{Si})_{i+1} = n(\text{Si})_i + \Delta t \left[\frac{dn(\text{Si})}{dt} \right]_{\text{tot},i}^{m,c} \quad (\text{B.9})$$

where $\Delta t = (t_{i+1} - t_i)$. In this case, the flow time at the slab of material $i + 1$, t_{i+1} , is numerically calculated as in Appendix A (see Eq. A.7), but using the function $f(z_i)$ defined as (see Sec. 2):

$$f(z_i) = \frac{1}{v_s - v_n(z_i)} \quad (\text{B.10})$$

The fractional abundance of silicon, H_2O and CH_3OH , is finally derived by doing $\chi(m) = n(m)/n(\text{H}_2)$ in each slab of material.

References

- Anders, E., & Grevesse, N. 1989, *Geochimica et Cosmochimica Acta*, 53, 197
- Benedettini, M., Viti, S., Giannini, T., Nisini, B., Goldsmith, P. F., & Saraceno, P. 2002, *A&A*, 395, 657
- Cabrit, S., Flower, D. R., Pineau des Forêts, G., le Bourlot, J., & Ceccarelli, C. 2004, *Ap&SS*, 292, 501
- Caselli, P., Hartquist, T. W., & Havnes, O. 1997, *A&A*, 322, 296
- Chapman, J. F., & Wardle, M. 2006, *MNRAS*, 371, 513
- Chièze, J.-P., Pineau des Forêts, G., & Flower D. R. 1998, *MNRAS*, 295, 672
- Dopita, M. A., & Sutherland, R. S. 2003, in *Astrophysics of the Diffuse Universe* (Berlin, New York: Springer), p. 212
- Draine, B. T. 1995, *Ap&SS*, 233, 111
- Draine, B. T., & Salpeter, E. E. 1979, *ApJ*, 231, 77
- Draine, B. T., Roberge, W. G., & Dalgarno, A. 1983, *ApJ*, 264, 485
- Falle, S. A. E. G. 2003, *MNRAS*, 344, 1210
- Field, D., May, P. W., Pineau des Forêts, G., & Flower, D. R. 1997, *MNRAS*, 285, 839
- Flower, D. R., Pineau des Forêts, G., Field, D., & May, P. W. 1996, *MNRAS*, 280, 447
- Flower, D. R., & Pineau des Forêts, G. 2003, *MNRAS*, 343, 390
- Girart, J. M., & Acord, J. M. P. 2001, *ApJ*, 552, L63
- Graedel, T. E., Langer, W. D., & Frerking, M. A. 1982, *ApJS*, 48, 321
- Herbst, E., & Leung, C. M. 1989, *ApJS*, 69, 271
- Jiménez-Serra, I., Martín-Pintado, J., Rodríguez-Franco, A., & Marcelino, N. 2004, *ApJ*, 603, L49
- Jiménez-Serra, I., Martín-Pintado, J., Rodríguez-Franco, A., & Martín, S. 2005, *ApJ*, 627, L121
- Kaufman, M. J., & Neufeld, D. A. 1996, *ApJ*, 456, 250
- Le Bourlot, J., Pineau des Forêts, G., Flower, D. R., & Cabrit, S. 2002, *MNRAS*, 332, 985
- Lesaffre, P., Chièze, J.-P., Cabrit, S., & Pineau des Forêts, G. 2004, *A&A*, 427, 147
- Martín-Pintado, J., Bachiller, R., & Fuente, A. 1992, *A&A*, 254, 315
- May, P. W., Pineau des Forêts, G., Flower, D. R., Field, D., Allan, N. L., & Purton, J. A. 2000, *MNRAS*, 318, 809
- Neufeld, D. A., Snell, R. L., Ashby, M. L. N., et al. 2000, *ApJ*, 539, L107
- Pilipp, W., Hartquist, T. W., & Havnes, O. 1990, *MNRAS*, 243, 685
- Pilipp, W., & Hartquist, T. W. 1994, *MNRAS*, 267, 801
- Pineau des Forêts, G., Flower, D. R., & Chièze, J.-P. 1997, in *Herbig-Haro Flows and the Birth of Stars*, IAU Symposium No. 182, Ed. B. Reipurth & C. Bertout (Kluwer Academic Publishers), p. 199-212.
- Prasad, S. S., & Huntress, W. T. Jr. 1982, *ApJ*, 260, 590
- Requena-Torres, M. A., Marcelino, N., Jiménez-Serra, I., Martín-Pintado, J., Martín, S., & Mauersberger, R. 2007, *ApJ*, 655, L37
- Smith, M. D., & Brand, P. W. J. L. 1990, *MNRAS*, 242, 495
- Smith, M. D., Brand, P. W. J. L., & Moorhouse, A. 1991, *MNRAS*, 248, 730
- Snow, T. P., & Witt, A. N. 1996, *ApJ*, 468, L65
- Tielens, A. G. G. M., & Allamandola, L. J. 1987, in *Physical Processes in Interstellar Clouds*, ed. G. E. Morfill & M. Scholer (Dordrecht: Reidel), p. 333
- Tielens, A. G. G. M., McKee, C. F., Seab, C. G., & Hollenbach, D. J. 1994, *ApJ*, 431, 321
- Whittet, D. C. B., & Duley, W. W. 1991, *A&A Rev.*, 2, 167
- Ziurys, L. M., Friberg, P., & Irvine, W. M. 1989, *ApJ*, 343, 201